Full length article

Direct observation of weakened interface clamping effect enabled ferroelastic domain switching

Mingqiang Li [a, b, c], Bo Wang [d], Heng-Jui Liu [e], Yen-Lin Huang [f], Jingmin Zhang [a], Xiumei Ma [a], Kaihui Liu [c, g, h], Dapeng Yu [a, g, h, i], Ying-Hao Chu [f, j], Long-Qing Chen [d], Peng Gao [a, b, c, g, *]

[a] Electron Microscopy Laboratory, School of Physics, Peking University, Beijing, 100871, China
[b] International Center for Quantum Materials, Peking University, Beijing, 100871, China
[c] Academy for Advanced Interdisciplinary Studies, Peking University, Beijing, 100871, China
[d] Department of Materials Science and Engineering, The Pennsylvania State University, University Park, PA, 16802, United States
[e] Department of Materials Science and Engineering, National Chung Hsing University, Taichung, 40227, Taiwan, ROC
[f] Department of Materials Science and Engineering, National Chiao Tung University, Hsinchu, 30010, Taiwan, ROC
[g] Collaborative Innovation Centre of Quantum Matter, Beijing, 100871, China
[h] State Key Laboratory for Mesoscopic Physics, School of Physics, Peking University, Beijing, 100871, China
[i] Department of Physics, South University of Science and Technology of China, Shenzhen, 518055, China
[j] Institute of Physics, Academia Sinica, Taipei 11529, Taiwan, ROC

ABSTRACT

Reversible switching of non-180° ferroelastic domains that largely alters the local strain distribution enables many electromechanical, electromagnetic and electroacoustic applications. However, in thin films, the ferroelastic domain walls are usually believed to be immobile because of the interface clamping and/or dislocation pinning. Here, using *in situ* and aberration-corrected transmission electron microscopy, we directly observe reversible switching of individual 90° domains in dislocation-free $PbTiO_3$ thin films and uncover the weakened interface clamping effect. We find the tetragonality is suppressed to ~1.017 while the polarization vectors rotate 45° in the *a*-domain near the interface. These huge structural distortions at the interface is mainly responsible for the weakened clamping effect and thus the ability to switch ferroelastic domains. The switching is fully reversible (i.e., either electric field or mechanical stress can re-establish the erased domain) regardless of polarization orientation of the *c*-domain matrix. Phase-field modeling also shows excellent agreement with experimental observations. Our study reveals the mechanism of controllable and reversible ferroelastic domain switching, enabling the design of new actuators, sensors, and electromagnetic devices.

© 2019 Acta Materialia Inc. Published by Elsevier Ltd. All rights reserved.

1. Introduction

In ferroelectrics, ferroelastic domain walls are characterized by a rotation of both crystallographic unit cells and polarization directions. The intrinsic coupling between strain and polarization charge of ferroelastic domains results in numerous interesting phenomena and unique applications in actuators, sensors, and nanoelectronics [1—6]. These applications usually appreciate the ability to manipulate ferroelastic domains under external stimuli,

i.e., mobile ferroelastic domain walls can significantly enhance the dielectric permittivity and piezoelectric response of ferroelectric materials [7—9], and switching of ferroelastic domains is vital in manipulating magnetoelectric coupling along multiferroic heterointerfaces [10,11].

However, ferroelastic domains in thin films are usually not switchable due to the interface clamping and/or dislocation pining [10,12—15]. The latter can be understood by the fact of a strong coupling between the ferroelastic domain walls and the intrinsic strain fields induced by dislocations [12,14]. Since dislocations are typically inactive under electric fields, the motion of dislocation pinned ferroelastic domain walls requires atom rearrangement, and is thus energetically costly and very difficult [13]. Indeed, the

electron microscopy studies confirmed that in most Pb(Zr, Ti)O$_3$ thin films edge dislocations are observed near 90° domain walls [14,16], and these domain walls are immobile under an electric field [17]. Although a reversible switching of needle-like ferroelastic domains was demonstrated in thin films [5,16], such switching behavior is only spring-like, i.e., after removal of the external fields, the needle-like ferroelastic domain returns to the initial state because a moderate external field cannot overcome the pinning from dislocations [16].

The effect of interface clamping on mobility and immobility of ferroelastic domain walls, is still not well understood. Many studies demonstrated that the interface between ferroelectrics and substrates hinders the ferroelastic domain wall motion [15,18,19], and it is believed that a huge strain redistribution is required at the ferroelectric-substrate interface during switching of ferroelastic domains, which should also be energetically expensive and unfavorable. Nevertheless, a few recent works reported mobile ferroelastic domains in dislocation-free PbTiO$_3$ films on a DyScO$_3$ substrate could be erased and created by an electric field [9,20,21] even without any energetically active needle-point (that plays a critical role in the nucleation of ferroelastic domains [16]). These results indicate that the interface clamping may be not as strong as the commonly believed, and the underlying mechanism for ferroelastic domain switching remains unclear, which motivates the present study of probing the atomic structure evolution during ferroelastic domain switching in ferroelectric thin films.

Here, we directly observe the reversible switching process of an individual ferroelastic domain and demonstrate the weakened interface clamping at atomic scale by combining the *in situ* transmission electron microscopy (TEM) probe technique [22–24], with quantitative image analysis [25,26]. We provide direct evidence for reversible ferroelastic domain switching under external electric fields in PbTiO$_3$ films regardless the polarization orientation of the *c*-domain matrix (*c*-domains possess polarization oriented out of the plane of the film; while *a*-domains, also known as ferroelastic domains possess polarization oriented in the plane of the film). The atomically mapped polarization shows that the polar vectors near the interface in the *a*-domain are rotated ~45° deviating from the equilibrium orientation, while the tetragonality of the *a*-domain becomes significantly suppressed to ~1.017 at the interface compared to 1.055 in the interior. We also performed phase-field simulations which are in excellent agreement with experimental observations and the results suggest that the rotated polarization at the interface originates from anisotropic in-plane misfit strain. Such an interfacial layer with a huge structure distortion acts as an intermediate zone to adopt a dramatic strain change across the interface, eliminating strong clamping effects of the interface on the ferroelastic domain switching. Moreover, the switching of ferroelastic domains is fully reversible, i.e., either an electric field or a mechanical stress can re-establish the erased ferroelastic domains. Our study clarifies the effects of the interface on ferroelastic domain switching and reveals the mechanism of domain wall motion. The ability to reversibly switch ferroelastic domains is believed to enhance the electromechanical response and enables new functional devices such as actuators and sensors.

2. Experimental procedures

2.1. Preparation of PbTiO$_3$ films

The 100-nm-thick PbTiO$_3$ thin films were grown on single crystal (110)o DyScO$_3$ substrates buffered with ~50-nm-thick SrRuO$_3$ electrodes using pulsed laser deposition method. A KrF excimer laser ($\lambda = 248$ nm) was focused on the targets with an energy density of ~2.5 mJ/cm^2 and repetition rate of 10 Hz. During the growth of the SrRuO$_3$, the temperature and the oxygen pressure were kept at 700 °C and 100 mTorr, respectively. To avoid the easy evaporation of the lead in PbTiO$_3$ thin film at high temperature, the target with 5% excess lead was used and the temperature for the subsequent growth of PbTiO$_3$ thin film was decreased to 650 °C at the same oxygen atmosphere. After the deposition process, an *in situ* post annealing process with the same temperature and high oxygen pressure environment of ~300 Torr for 30 min was adopted to effectively eliminate the oxygen vacancies of the sample. Finally, the sample was slowly cooled down to room temperature with a ramp rate of 5 °C/min.

2.2. TEM sample preparation and TEM test

The cross-sectional TEM samples were prepared by conventional mechanical polishing and followed by argon ion milling in a Precision Ion Polishing System 691 (Gatan). Ion milling procedure consists of two steps. In the first stage of coarse milling, the guns were at 4 keV with angles 6° and −6°. In the following condition, the guns were set at 1 keV for 5 min with angles of 3° and −3°, and further lowered to 0.1 keV for 2 min for final surface cleaning. Diffraction contrast TEM experiments were carried out using Tecnai F20 microscope (FEI) where samples were tilted off the zone axis and imaged in the bright field or dark field with two-beam alignment condition using a (200) g vector. High-angle annular dark field (HAADF) images used in this work were obtained from an aberration-corrected FEI Titan Themis G2 microscope operating at 300 kV. Atom positions were determined by simultaneously fitting two-dimensional Gaussian peaks to a perovskite unit cell using a home-developed code running in MatLab R2011a. Polar displacements of the Pb cations were measured relative to the centre of the surrounding Ti cations in HAADF-STEM images. Geometric phase analysis (GPA) was performed using a free FRWRtools plugin for Digital Micrograph based on the original work by Hÿtch et al. [27].

2.3. Phase-field simulations

The phase-field method has been extensively used to model domain formation and transition under external stimuli in various ferroelectric systems [28]. The temporal evolution of polarization vector field **P** is obtained by solving the time-dependent Ginzburg-Landau (TDGL) equation, i.e.,

$$\frac{\partial P_i}{\partial t} = -L \frac{\delta F}{\delta P_i}, i = 1, 2, 3 \tag{1}$$

where F is the volume integral of the total free energy of the system consisting of contributions from bulk, elastic, electric, and gradient energies. Explicit expressions of each term in F can be found in our previous works [29,30]. The TDGL equation is solved in a semi-implicit Fourier spectral framework using a discrete grid of 128 $\Delta x \times 1 \Delta x \times 128 \Delta x$ where the grid spacing $\Delta x = 1$ nm. Periodical boundary conditions are adopted along the x_1 and x_2 axes in the lateral directions of films while appropriate boundary conditions for elastic and electrical equilibrium equations along the x_3 axes in the out-of-plane direction, as described in detail in our previous publications [29,30]. A thickness of 100 Δx was used to model the film while 20 Δx to relax the mechanical displacement into the substrate.

3. Results

3.1. Ferroelastic domain switching

The 100-nm-thick PbTiO$_3$ thin films were deposited on single

crystal substrates DyScO$_3$ (100)o (the subscript O indicates ortho-rhombic) which possesses a slight lattice mismatch (~1%) with PbTiO$_3$ [31–34]. A 50-nm-thick SrRuO$_3$ acts as the bottom electrode. Fig. 1a shows a typical *a/c* domain pattern in PbTiO$_3$ films. The polarization of embedded *a*-domains is nearly perpendicular to that of *c*-domains as schematically illustrated in Fig. 1b. The electron diffraction pattern confirms the lattice parameter ratio *c/a* is ~1.055 (Fig. S1). A typical chronological diffraction contrast TEM image series in Fig. 1c shows the switching process of a ferroelastic domain driven by a negative bias (the SrRuO$_3$ electrode is always grounded). The polarization of *c*-domain matrix in Fig. 1c is upward (Fig. S2 and Supplementary movie 1). For ferroelastic domains embedded within the downward *c*-domain matrix (Fig. S3), switching can also be achieved by applying a positive bias in Fig. 1d. We quantitatively measure the motion of ferroelastic domain walls. The width and length of *a*-domain are plotted as a function of applied voltage in Fig. 1e. The switching process of ferroelastic domains shows two stages apparently. The first stage is from 0 to 12 V in Fig. 1e during which the ferroelastic domain becomes narrower with the increase of the applied voltage. As it shown in Fig. 1e, the surface, middle and bottom width of the ferroelastic domain in Fig. 1c decrease at the same pace while the length of the domain keeps a constant of 140 nm. Unlike the motion of 180° domain walls that are usually curved and charged under the external electric field [35], 90° domain walls remain nearly straight and move in the opposite direction during switching. In the second stage, the domain length starts to decrease until the whole domain is switched under 13 V. This two-stage switching behavior is illustrated schematically in Fig. 1f. Although most annihilations of ferroelastic domain initially occur at the top surface (Fig. 1c and d) mainly owing to the stronger electric fields near the tip [35], eradicating from the bottom interface also have been captured from the same sample (Fig. S4). These results indicate the absence of a strong clamping at the interface, enabling the switching of ferroelastic domains.

Supplementary video related to this article can be found at https://doi.org/10.1016/j.actamat.2019.04.003.

3.2. Atomic structure of the *a*-domain

In order to reveal the mechanism of the absent strong clamping effect, atomically resolved *Z*-contrast HAADF images of the interface are analyzed. The calculated polarization vectors overlaid with the image are shown in Fig. 2a. No dislocation is observed at the interface. Unexpectedly, the 45° rotated polarization vector are revealed in *a*-domain (Fig. 2a and b), i.e., near the interface in *a*-domain (zone C), the polarization orientation significantly deviates from the symmetry permitted axis and rotates from $[100]_{pc}$ to $[10\bar{1}]_{pc}$ axis (pc denotes the pseudo-cubic structure). Polarization rotation of 10°–15° in the *c*-domain near ferroelastic domain walls driven by flexoelectric effect has been reported in a similar system [36,37]. Unlike the previous studies, in the present case nearly 45° polarization rotation at the *a*-domain is due to the anisotropic in-plane misfit strain (stems from the anisotropic in-plane lattice parameter of *a*-domain), as suggested by phase-field simulations (Fig. S5). The simulated polarization configuration in Fig. 2c shows that the out-of-plane polarization is reduced in magnitude and the polarization vector rotates toward direction at the left side (obtuse corner) of the *a*-domain which is in excellent agreement with the experimental observations.

The in-plane and out-of-plane lattice parameters are also mapped at the unit cell scale and carefully calibrated as described in Table S1 and Fig. S6 to reveal the strain distribution at the interface. In the *a*-domain, the in-plane lattice parameter is significantly suppressed near the interface in Fig. 2d while the out-of-plane lattice parameter almost remains unchanged in Fig. 2e, and thus the tetragonality is reduced to ~1.017 near the interface in Fig. 2f. The thickness of the interfacial region with a suppressed tetragonality is ~14 unit cells, wherein the lattice *c* (in-plane) is gradually reduced from 415 pm to 402 pm at the interface in Fig. 2g. The compression of lattice *c* arises from that DyScO$_3$ has smaller in-
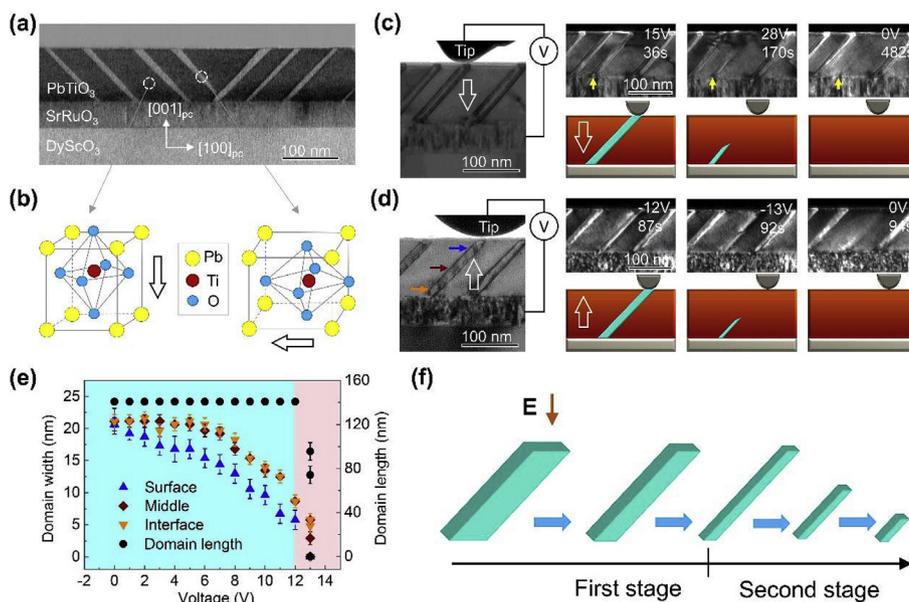
Fig. 1. Domain structure and electric field induced switching of an individual *a*-domain. (a) A STEM image of PbTiO$_3$ thin films grown on DyScO$_3$ with 50-nm-thick SrRuO$_3$ electrodes. (b) Schematics of the unit cells in *c*-domain with out-of-plane polarization and in *a*-domain with in-plane polarization. (c) A chronological TEM dark-field image series depicting the switching process of an *a*-domain under negative voltage. (d) A chronological TEM dark-field image series depicting the switching process of an *a*-domain under positive voltage. The SrRuO$_3$ electrode is grounded. (e) The width and length of *a*-domain as a function of applied voltage. The width of *a*-domain in the bottom, middle and surface corresponding to the three marked arrows in (c). The dark circle shows the length of *a*-domain. (f) Schematic illustration of the two-stage switching process of an individual ferroelastic domain driven by electric fields.
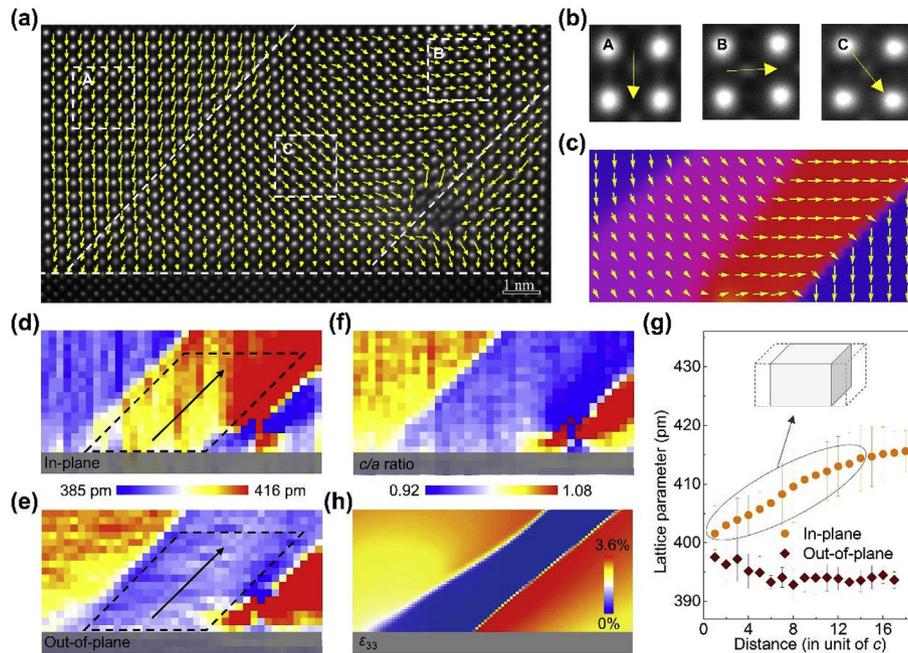
Fig. 2. Atomic structure of the *a*-domain. (a) An atomically resolved HAADF-STEM image of an *a*-domain in PbTiO₃ films overlaid with atomic displacement vectors. (b) Enlarged PbTiO₃ unit cells are averaged from the three marked areas in (a). (c) Phase-field modeling of polarization arrangements of the *a*-domain. (d) In-plane, (e) out-of-plane lattice parameters, and (f) *c/a* ratio maps of *c/a/c* domains. The SrRuO₃ electrode is indicated by a gray rectangular. (g) Profiles of the in-plane and out-of-plane lattice parameters in *a*-domain corresponding to the marked areas in (c) and (d). The inset indicates the reduced lattice *c* in *a*-domain. The error bar is the standard deviation (s.d.). (h) Simulate out-of-plane normal strain around the *a*-domain.

plane lattice parameters (396 pm) compared with the lattice *c* of the *a*-domain in PbTiO₃ (416 pm) [31–34]. In addition, the lattice distortion also occurs in the *c*-domains. In Fig. 2e, the out-of-plane lattice parameter of the left *c*-domain is compressed while the right one is elongated which is further confirmed by GPA in Fig. S7. The simulated out-of-plane normal strain distribution in Fig. 2h also illustrates the opposite states of strain near the two ferroelastic domain walls, which matches well with experimental observations.

3.3. Atomic structure of the interface before and after switching

To further reveal the switching characters at an atomic scale, we perform quantitatively comparison of the atomic structure at the interface before (Fig. 3a) and after (Fig. 3b) switching. Both the out-of-plane (Fig. 3c and d) and in-plane (Fig. 3e and f) lattice parameters are mapped respectively. The out-of-plane lattice parameter is suppressed in the first 12 unit cells in *c*-domain (left-hand side of the *a*-domain) and the reduction of tetragonality is up to 4.2%, as shown in the marked area in Fig. 3c. The out-of-plane lattice parameter of the same area is shown in Fig. 3d after switching, which shows the interfacial layer with suppressed tetragonality completely disappeared when the ferroelastic domain is switched, i.e., the as-grown out-of-plane lattice parameter near the interface is ~402 pm before switching while it becomes ~415 pm after switching in Fig. 3g. Meanwhile, in Fig. 3h the in-plane lattice parameter in the neighboring *c*-domain slightly increases (~0.3%) after switching because the in-plane lattice parameter in the *a*-domain region is reduced from pristine lattice *c* to final lattice *a* after switching. The same conclusion is further confirmed by the GPA data (Fig. S8).

### 3.4. Re-establishment of the a-domain by electric and mechanical field

Switching of ferroelastic domains is fully reversible under either an external electric field or a mechanical stress. An *a*-domain is firstly erased by an electrical bias (Fig. 1d) and it does not come back when the voltage is turned off (Fig. 4a). However, once the applied voltage is reversed, it can be switched back as shown in Fig. 4b (Supplementary movie 2). Besides electric fields, the mechanical stress can also bring an erased *a*-domain back. Fig. 4c shows that the *a*-domain is initially erased electrically as shown in Fig. 1c. In Fig. 4d, the probe acts as an indenter to impose force on the top of the films and then the ferroelastic domain appears suddenly. Lattice rotation maps of the pristine (Fig. 4e), switched (Fig. 4f) and recovered (Fig. 4g) states of the *a*-domain are analyzed for comparison. Profiles of lattice rotation in Fig. 4h shows that the recovered *a*-domain is almost identical to the pristine state except for a slight shrinkage from as-grown 43 to 37 unit cells in width. Furthermore, the recovered *a*-domain can be switched again under applied bias (Fig. S9).

Supplementary video related to this article can be found at https://doi.org/10.1016/j.actamat.2019.04.003.

4. Discussion

Although a certain degree of manipulation of ferroelastic domains in thin films has been achieved and it is already well accepted that the dislocations show strong pining effects on ferroelastic domains motion [12–14], previous studies have not reached an agreement regarding the effects of interface clamping on the domain wall mobility, and the underlying mechanisms that determine the mobility or immobility of ferroelastic domains remains controversial and elusive [4,5,38,39]. From our results, the mobility of ferroelastic domains in the dislocation-free PbTiO₃ film originates from the naturally weakened strength of clamping effect from the interface. Based on the *c/a* ratio, a ~12.4% change in strain distribution is expected at the ferroelectric-substrate interface during switching of ferroelastic domains. In this case, the switching
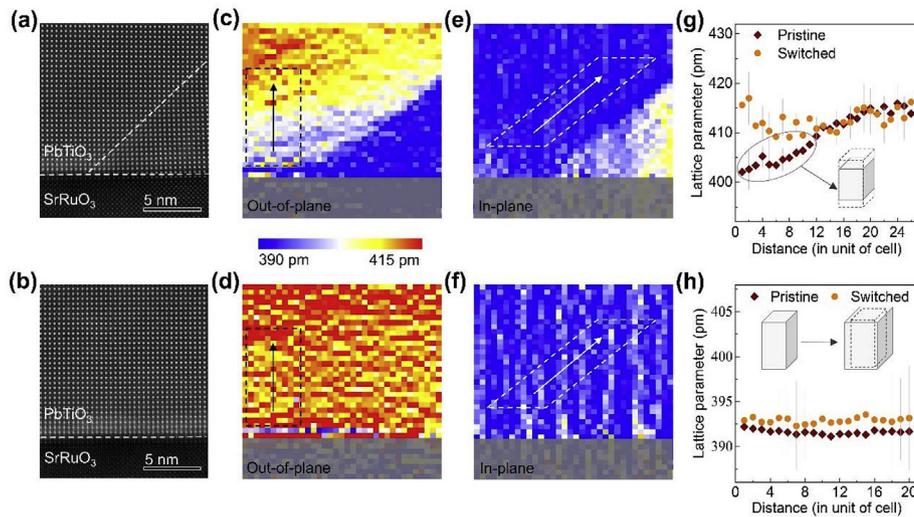
Fig. 3. Atomic structure evolution of the interface during switching. (a) and (b) Atomically resolved HAADF-STEM images of the same area at PbTiO$_3$/SrRuO$_3$ interface before switching (a) and after switching (b). The dashed lines indicate the interface and ferroelastic domain walls. (c) and (d) The corresponding out-of-plane lattice parameter maps for (a) and (b) respectively. The SrRuO$_3$ electrode is indicated by a gray rectangular. (e) and (f) The corresponding in-plane lattice parameter maps for (a) and (b) respectively. (g) Profiles of the out-of-plane lattice parameter corresponding to the marked areas in (c) and (d). The schematic illustrates the change of a single unit cell. (h) Profiles of the in-plane lattice parameter corresponding to the marked area along the domain wall in (e) and (f). The schematic illustrates the change of a single unit cell.
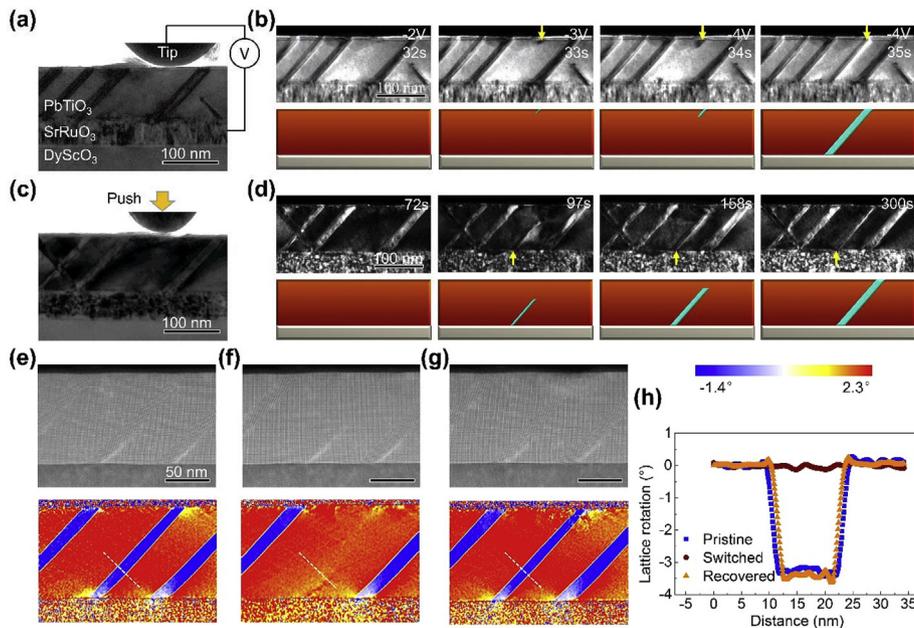
Fig. 4. Recovery of *a*-domains via electrical and mechanical stimuli. (a) A bright field TEM image of the domain structure. (b) A chronological image series showing the recovery process of *a*-domain by electric fields with schematics. (c) A bright field TEM image of the domain structure. The W tip acts as an indenter for mechanical loading. (d) A chronological image series showing the recovery of *a*-domain under mechanical excitation with schematics. HAADF-STEM images of the pristine (e), switched (f) and recovered (g) states of *a*-domain with lattice rotation maps obtained from GPA indicate the locally reversible switching of the individual *a*-domain. (h) Profiles of lattice rotation corresponding to the dashed lines in lattice rotation maps. The lattice rotation in *c*-domain far away from the domain wall is normalized to 0.

process is presumed to be energetically costly and thus unfavorable. However, our study shows that the clamping effect is not as strong as the fundamental belief due to complicated structure distortion near the interface. Firstly, the atomically mapped strain distribution shows the in-plane lattice parameter gradually decreases from 14th unit cell away from the interface. In this scenario, only a slight change (~2.6%) is required at the interface during ferroelastic domain switching. Besides the reduction of tetragonality, the polar vectors deviating from the permitted <001> axis of tetragonal phase should also be energetically active as the first

principle calculations [4] suggests the most stable polar vectors in the tetragonal phase should along <001> axis. The electric field maps in PbTiO$_3$ films are provided in Fig. S10. These factors together weaken the clamping effect, enabling reversible switching of ferroelastic domains.

The previously reported switching phenomena of ferroelastic domains in tetragonal thin films are usually accompanied by the 180° switching [7,21,40]. Such switching behavior is usually irreversible and complicated, i.e., electric fields can sometimes erase the ferroelastic domains but fail to bring them back after reversing

the external voltage [21,41]. In the present study, no 180° ferro-electric switching is needed for ferroelastic domain switching. The reversible switching of *a*-domain by electric fields can be understood by phenomenological energy barrier type model [20]. Switching results in the increase of the in-plane lattice parameter in the *c*-domain as shown in Fig. 3, while during back-switching by applying a proper stimulus (i.e., reversed electric field or strain field), the *c*-domains release their stored elastic energy, bringing the *a*-domain back. Note that the *a*-domains embedded in both of downward and upward *c*-domains can be switched which is important for practical applications.

The ability to controllably and reversibly switch of ferroelastic domains enables many functions. For example, given 1.055 *c/a* ratio of the PbTiO₃ unit cell, the electromechanical response would be comparable to or even more significant than piezoelectrically induced strain [42,43] if a significant volume fraction of the ferroelectric film could undergo a ferroelastic transition from *a* to *c* orientations. Due to the enhanced conductivity of ferroelastic domain walls [6], the mobile, writeable, and erasable ferroelastic domain walls can be used as nanoscale electronic elements for memories and logic devices. Furthermore, since the ferroelastic domains also play key roles in the magneto-electric coupling multiferroic materials and heterostructures [10,11], the switching of ferroelastic domains enables manipulation of magnetic properties via electric fields or mechanical stress.

5. Conclusion

In summary, direct observations of reversible 90° ferroelastic domain switching in PbTiO₃ films is presented and the underlying mechanism of domain wall mobility is revealed by *in situ* and aberration-corrected TEM combined with phase-field modeling. We find that the switchability of the ferroelastic domains originates from the dislocation-free quality of the film and weakened strength of interface clamping due to the hugely distorted structure, i.e., polarization rotation and significantly reduced tetragonality in *a*-domain. Phase-field simulation precisely reproduces the polarization rotation and strain distribution. The switching is fully reversible regardless of polarization orientation in the *c*-domain matrix, and either electrical or mechanical stimuli can bring the erased domain back. The atomic structure evolution during ferroelastic switching indicates that the interface clamping is not so strong as the fundamental belief, thus clarifying the controversy in previous experimental observations. The ability to controllably and reversibly switch ferroelastic domains offers new insights for applications of ferroelectric thin films in nanosized multifunctional devices.

Appendix A. Supplementary data

References

[1] J. Scott, Science 315 (2007) 954.
[2] G. Catalan, J. Seidel, R. Ramesh, J.F. Scott, Rev. Mod. Phys. 84 (2012) 119.
[3] L.W. Martin, A.M. Rappe, Nat. Rev. Mater. 2 (2016) 16087.
[4] B. Meyer, D. Vanderbilt, Phys. Rev. B 65 (2002).
[5] J.C. Agar, A.R. Damodaran, M.B. Okatan, J. Kacher, C. Gammer, R.K. Vasudevan, S. Pandya, L.R. Dedon, R.V. Mangalam, G.A. Velarde, S. Jesse, N. Balke, A.M. Minor, S.V. Kalinin, L.W. Martin, Nat. Mater. 15 (2016) 549.
[6] X.K. Wei, T. Sluka, B. Fraygola, L. Feigl, H. Du, L. Jin, C.L. Jia, N. Setter, ACS Appl. Mater. Interfaces 9 (2017) 6539.
[7] V. Nagarajan, A. Roytburd, A. Stanishevsky, S. Prasertchoung, T. Zhao, L. Chen, J. Melngailis, O. Auciello, R. Ramesh, Nat. Mater. 2 (2003) 43.
[8] J. Karthik, A.R. Damodaran, L.W. Martin, Phys. Rev. Lett. 108 (2012) 167601.
[9] A.R. Damodaran, S. Pandya, J.C. Agar, Y. Cao, R.K. Vasudevan, R. Xu, S. Saremi, Q. Li, J. Kim, M.R. McCarter, L.R. Dedon, T. Angsten, N. Balke, S. Jesse, M. Asta, S.V. Kalinin, L.W. Martin, Adv. Mater. 29 (2017) 1702069.
[10] S. Baek, H. Jang, C. Folkman, Y. Li, B. Winchester, J. Zhang, Q. He, Y. Chu, C. Nelson, M. Rzchowski, Nat. Mater. 9 (2010) 309.
[11] Y.-H. Chu, L.W. Martin, M.B. Holcomb, M. Gajek, S.-J. Han, Q. He, N. Balke, C.-H. Yang, D. Lee, W. Hu, Nat. Mater. 7 (2008) 478.
[12] M.W. Chu, I. Szafraniak, R. Scholz, C. Harnagea, D. Hesse, M. Alexe, U. Gosele, Nat. Mater. 3 (2004) 87.
[13] I. Vrejoiu, G. Le Rhun, N.D. Zakharov, D. Hesse, L. Pintilie, M. Alexe, Philos. Mag. A 86 (2006) 4477.
[14] D. Su, Q. Meng, C.A.F. Vaz, M.-G. Han, Y. Segal, F.J. Walker, M. Sawicki, C. Broadbridge, C.H. Ahn, Appl. Phys. Lett. 99 (2011) 102902.
[15] F. Griggio, S. Jesse, A. Kumar, O. Ovchinnikov, H. Kim, T.N. Jackson, D. Damjanovic, S.V. Kalinin, S. Trolier-McKinstry, Phys. Rev. Lett. 108 (2012) 157604.
[16] P. Gao, J. Britson, C.T. Nelson, J.R. Jokisaari, C. Duan, M. Trassin, S.H. Baek, H. Guo, L. Li, Y. Wang, Y.H. Chu, A.M. Minor, C.B. Eom, R. Ramesh, L.Q. Chen, X. Pan, Nat. Commun. 5 (2014) 3801.
[17] J. Britson, C. Nelson, X. Pan, L.-Q. Chen, Acta Mater. 75 (2014) 188.
[18] L. Feigl, P.E. Janolin, T. Yamada, M. Iwanowska, C.S. Sandu, N. Setter, Appl. Phys. Lett. 106 (2015), 032902.
[19] T. Shaw, S. Trolier-McKinstry, P. McIntyre, Annu. Rev. Mater. Sci. 30 (2000) 263.
[20] A.I. Khan, X. Marti, C. Serrao, R. Ramesh, S. Salahuddin, Nano Lett. 15 (2015) 2229.
[21] L. Feigl, L.J. McGilly, C.S. Sandu, N. Setter, Appl. Phys. Lett. 104 (2014) 172904.
[22] Y. Tang, Y. Zhu, X. Ma, A.Y. Borisevich, A.N. Morozovska, E.A. Eliseev, W. Wang, Y. Wang, Y. Xu, Z. Zhang, Science 348 (2015) 547.
[23] Y.M. Kim, J. He, M.D. Biegalski, H. Ambaye, V. Lauter, H.M. Christen, S.T. Pantelides, S.J. Pennycook, S.V. Kalinin, A.Y. Borisevich, Nat. Mater. 11 (2012) 888.
[24] M.G. Han, M.S. Marshall, L. Wu, M.A. Schofield, T. Aoki, R. Twesten, J. Hoffman, F.J. Walker, C.H. Ahn, Y. Zhu, Nat. Commun. 5 (2014) 4693.
[25] C.L. Jia, S.B. Mi, K. Urban, I. Vrejoiu, M. Alexe, D. Hesse, Nat. Mater. 7 (2008) 57.
[26] A.B. Yankovich, B. Berkels, W. Dahmen, P. Binev, S.I. Sanchez, S.A. Bradley, A. Li, I. Szlufarska, P.M. Voyles, Nat. Commun. 5 (2014) 4155.
[27] M. Hýtch, E. Snoeck, R. Kilaas, Ultramicroscopy 74 (1998) 131.
[28] L.-Q. Chen, J. Am. Ceram. Soc. 91 (2008) 1835.
[29] Y. Li, S. Hu, Z. Liu, L. Chen, Acta Mater. 50 (2002) 395.
[30] Y.L. Li, S.Y. Hu, Z.K. Liu, L.Q. Chen, Appl. Phys. Lett. 81 (2002) 427.
[31] J. Haeni, P. Irvin, W. Chang, R. Uecker, P. Reiche, Y. Li, S. Choudhury, W. Tian, M. Hawley, B. Craigo, Nature 430 (2004) 758.
[32] S. Zhang, Y. Zhu, Y. Tang, Y. Liu, S. Li, M. Han, J. Ma, B. Wu, Z. Chen, S. Saremi, X. Ma, Adv. Mater. 29 (2017) 1703543.
[33] M. Biegalski, J. Haeni, S. Trolier-McKinstry, D. Schlom, C. Brandle, A.V. Graitis, J. Mater. Res. 20 (2005) 952.
[34] Y. Kuroiwa, S. Aoyagi, A. Sawada, J. Harada, E. Nishibori, M. Takata, M. Sakata, Phys. Rev. Lett. 87 (2001) 217601.
[35] P. Gao, C.T. Nelson, J.R. Jokisaari, S.-H. Baek, C.W. Bark, Y. Zhang, E. Wang, D.G. Schlom, C.-B. Eom, X. Pan, Nat. Commun. 2 (2011) 591.
[36] G. Catalan, A. Lubk, A.H. Vlooswijk, E. Snoeck, C. Magen, A. Janssens, G. Rispens, G. Rijnders, D.H. Blank, B. Noheda, Nat. Mater. 10 (2011) 963.
[37] Y. Cao, L.-Q. Chen, S.V. Kalinin, Appl. Phys. Lett. 110 (2017) 202903.
[38] C.S. Ganpule, V. Nagarajan, H. Li, A.S. Ogale, D.E. Steinhauer, S. Aggarwal, E. Williams, R. Ramesh, P. De Wolf, Appl. Phys. Lett. 77 (2000) 292.
[39] R. Xu, S. Liu, I. Grinberg, J. Karthik, A.R. Damodaran, A.M. Rappe, L.W. Martin, Nat. Mater. 14 (2015) 79.
[40] L. Chen, J. Ouyang, C.S. Ganpule, V. Nagarajan, R. Ramesh, A.L. Roytburd, Appl. Phys. Lett. 84 (2004) 254.
[41] G.L. Rhun, I. Vrejoiu, L. Pintilie, D. Hesse, M. Alexe, U. Gösele, Nanotechnology 17 (2006) 3154.
[42] X. Ren, Nat. Mater. 3 (2004) 91.
[43] D. Damjanovic, Rep. Prog. Phys. 61 (1998) 1267.